Understanding the unusual stiffness of hydrophobic dipeptide crystals: supplementary information

Jorge M. del Campo[a] and Joel Ireta[b]

[a] Departamento de Física y Química Teórica, Facultad de Química, Universidad Nacional Autónoma de México, Ciudad de México, C.P. 04510, México; E-mail: jmdelc@unam.mx

[b] Departamento de Química, División de Ciencias Básicas e Ingeniería, Universidad Autónoma Metropolitana-Iztapalapa, A.P. 55-534, Ciudad de México 09340, México; E-mail: iret@xanum.uam.mx

The energy-strain method

In this section we reproduce the elastic constants results presented by Kronik *et al.* for the FF crystal. [1] For that we have employed the PBE functional with the iterative Tkatchenko-Scheffler dispersion corrections (TS-vdW), an energy-cuttoff of 1600 eV, a KPOINT mesh of 1x1x4 and the energy-strain methodology. The obtained lattice parameters and elastic constants for FF are presented in Table 1. We also listed the results reported by Kronik *et al.* As can be seen the previously reported results and the here obtained are in very good agreement.

Table 1: Computed lattice parameters (in Å), volume (in $\mathring{A}^3$), and the lattice parameter ratio comparison for FF dipeptide optimizaion with PBE-TS-vdW. As well as the elastic constants obtained with the energy-strain method.

	$\|\vec{a}\|$	$\|\vec{c}\|$	V_0	$\|\vec{c}\|/\|\vec{a}\|$
This work	23.94	5.39	2676.95	0.225
Previous work [1]	23.89	5.38	2659.16	0.225

Elastic Constants (in GPa), Poisson Ratio, and Young's Moduli (in GPa).

	C_{11}	C_{33}	C_{12}	C_{13}	ν_{12}	E_1	E_3
This work	17.47	25.43	11.10	11.00	0.50	9.55	16.95
Previous work [1]	17.56	24.05	11.91	11.00	0.54	8.75	15.85

The curve fitting plots used for obtaining the results presented in Table 1 are presented in Figure 1. In each plot it is indicate the combination of elastic constants associated to the energy response upon straining the system. In these plots can be observed that for all the applied strains the resulting energy change is marginal and lies in the precision range that DFT plane wave codes can predict, in particular, the plot associated to the C_{11}-C_{12} in which the maximum energy change amounts to 0.01 eV (0.23 kcal/mol) revealing that the potential energy surface for this particular system is fluxional. We consider that this low energy change makes the energy-strain methodology highly prone to convergence issues, as it has been thoroughly investigated by Caro *et al.* [2]

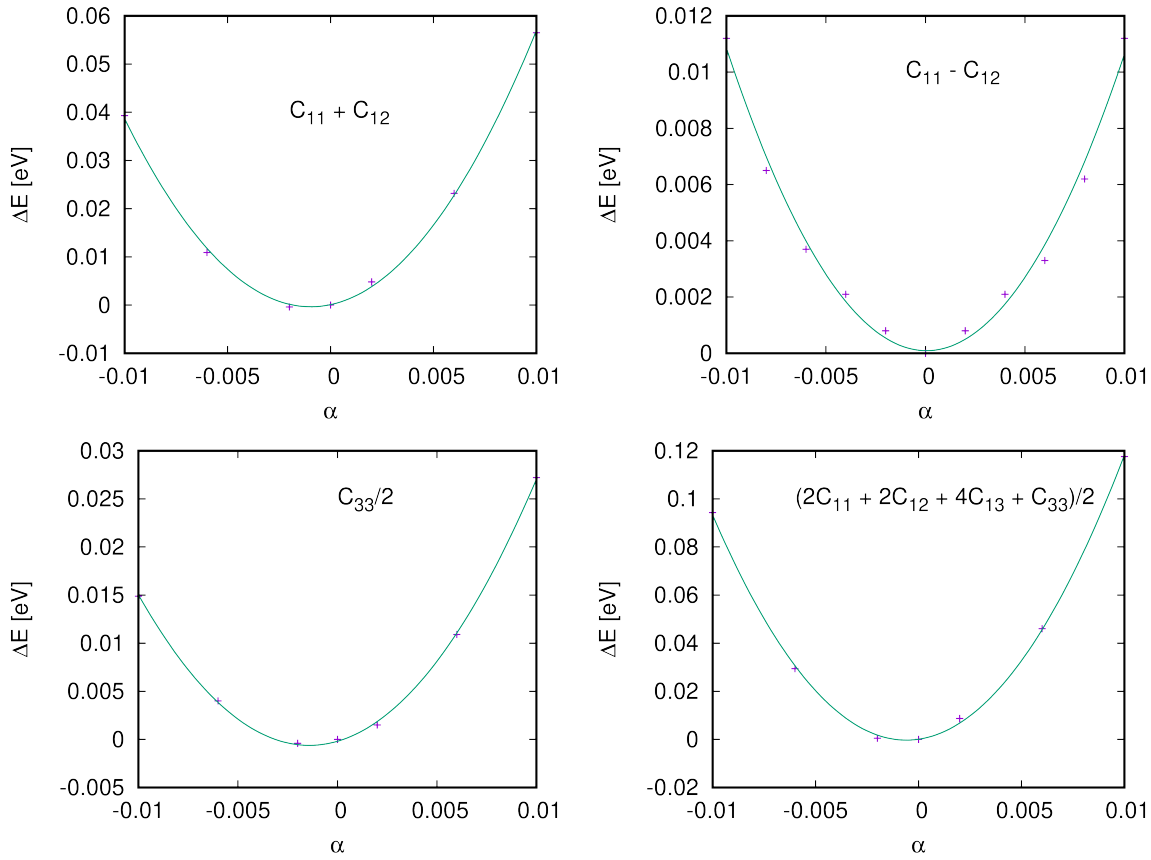

Figure 1: Energy curves, as a function of strain, computed with PBE and the iterative TS-vdW correction. Solid lines represent a parabolic fit and the elastic constant combination extracted from the curvature of each fit is denoted on each panel.

The stress-strain method

In this section detailed intermediate results are presented for the FF dipeptide crystal obtained with DFT. These DFT calculations are performed using the PBE functional with Tkatchenko-Scheffler dispersion corrections (TS-vdW), an energy-cuttoff of 1600 eV, a KPOINT mesh of 1x1x4, and the stress-strain methodology. Starting from a fully relaxed dipeptide crystal with a stress matrix converged to 10^{-2} kB:

$$s_0 = \begin{pmatrix} 0.07234797 & 0.00266576 & -0.00333445 \\ 0.00266576 & 0.05783309 & -0.00260705 \\ -0.00333445 & -0.00260707 & 0.05554635 \end{pmatrix}$$

we have computed the elastic matrix elements, C_{ij}, from stress-strain relations that allow us to extract individual elastic constants separately using single linear least-squares-fit to stress-strain relations. To provoke changes in the stress matrix we follow the methodology described by de Jong *et. al.* [3] in which it is employed a

Green-Lagrange strain tensor, $\mathbf{E}$, defined as:

$$\mathbf{E} = \frac{1}{2}(\delta^T \delta - \mathbf{I}) \tag{1}$$

where δ denotes the applied distortion matrix. The set of distorted structures is obtained using the open-source materials analysis code pymatgen [4] with distortion cell values $\alpha = \{-0.01, -0.0075 - 0.005, +0.005, +0.0075, +0.01\}$ for shear-modes and non shear-modes. Atom positions inside the distorted cell are optimized for obtaining the corresponding stress tensor. Three regression sets, $\epsilon_1 = \{-0.01, -0.005, +0.005, +0.01\}$, $\epsilon_2 = \{-0.005, +0.005\}$ and $\epsilon_3 = \{-0.0075, -0.005, +0.005, +0.0075\}$ are employed to check if the resulting bulk moduli are in agreement within 15%, as recommended, [3] in order to determine whether the range of strains considered is appropriate for deriving the elastic constant tensor using a linear stress-strain relationship. The compliance tensor, $\mathbf{s}$, is obtained by inverting the elastic matrix $\mathbf{C}$. Young's moduli are then calculated as, $E_i = 1/s_{ii}$, and the Poisson's ratios with the relation $\nu_{ij} = -s_{ij}/s_{ii}$. The linear least-squares-fit to stress-strain relations is carried out using Mathematica notebook. The following intermediate results are obtained for computing the C_{11}, C_{12}, C_{13} , C_{14}, C_{15} and C_{16} elastic constants if the ϵ_1 regression set is applied to strain the crystal with the next distortion matrix:

$$\boldsymbol{\delta} = \begin{pmatrix} 1+\epsilon_1 & 0 & 0 \\ 0 & 1 & 0 \\ 0 & 0 & 1 \end{pmatrix}$$

the corresponding calculated stress matrices are (in kB):

$$s_{\epsilon_1=-0.01} = \begin{pmatrix} 3.52767085 & 0.00295768 & -0.00291534 \\ 0.00295768 & 1.53984823 & 0.00020327 \\ -0.00291534 & 0.00020327 & 1.55326728 \end{pmatrix}$$

,

$$s_{\epsilon_1=-0.005} = \begin{pmatrix} 2.11368108 & 0.00853872 & -0.00271436 \\ 0.00853872 & 0.91087359 & 0.00027395 \\ -0.00271436 & 0.00027395 & 0.87185023 \end{pmatrix}$$

,

$$s_{\epsilon_1=+0.005} = \begin{pmatrix} -1.32651159 & 0.00801234 & -0.00249455 \\ 0.00801234 & -0.32350397 & 0.00014273 \\ -0.00249455 & 0.00014273 & -0.42458617 \end{pmatrix}$$

and

$$s_{\epsilon_1=+0.01} = \begin{pmatrix} -2.24861723 & 0.00688584 & -0.00234459 \\ 0.00688584 & -0.73727241 & -0.00005658 \\ -0.00234459 & -0.00005658 & -0.95986670 \end{pmatrix}$$

and the obtained C_{11}, C_{12}, C_{13} values are 29.9855, 11.5772 and 12.6454 GPa, respectively (C_{14}, C_{15} and C_{16},

as expected for the hexagonal FF crystal, are close to zero and could be discarded). In a similar way the ϵ_1 regression set is used to strain the system according to the next distortion matrix

$$\boldsymbol{\delta} = \begin{pmatrix} 1 & 0 & 0 \\ 0 & 1+\epsilon_1 & 0 \\ 0 & 0 & 1 \end{pmatrix}$$

for getting the C_{21}, C_{22}, C_{23} elastic constants. The obtained values are 11.7265, 30.8255 and 12.782 GPa, respectively. Finally, for the ϵ_1 regression set is used to strain the system with the next distortion matrix:

$$\boldsymbol{\delta} = \begin{pmatrix} 1 & 0 & 0 \\ 0 & 1 & 0 \\ 0 & 0 & 1+\epsilon_1 \end{pmatrix}$$

leading to C_{31}, C_{32}, C_{33} values of 12.8772, 12.8709 and 28.6398 GPa, respectively. The corresponding upper block **C** matrix

$$\begin{pmatrix} 29.9855 & 11.5772 & 12.6454 \\ 11.7265 & 30.8255 & 12.782 \\ 12.8772 & 12.8709 & 28.6398 \end{pmatrix} \tag{2}$$

obtained for the hexagonal FF crystal system is not symmetric, however the differences between the symmetry related elements are negligible. Upon inversion we get the next Young's Moduli, $E_1 = 22.9$ GPa and $E_2 = 23.6$ GPa for FF, values that correlate well with the reported experimental ones for such property.

To further corroborate the reliability of our results we have calculated the Poisson's ratios, ν_{ij}, which are within the theoretical bound $-1 < \nu_{ij} < 0.5$ (see Table 2). It is known that deviations from this bound are connected to the accumulation of numerical errors in the calculation of the elastic matrix elements. The values of the Poisson's ratios here calculated are indeed in the range from 0.09 to 0.45, giving us confidence in the methodology used for calculating the elastic matrix elements.

Table 2: Computed Poisson's Ratios

Dipeptide	ν_{12}	ν_{21}	ν_{13}	ν_{31}	ν_{23}	ν_{32}
FF	0.235	0.246	0.337	0.312	0.338	0.300
FF6N	0.206	0.206	0.376	0.311	0.383	0.309
LF-Water	0.318	0.251	0.170	0.127	0.288	0.356
LF-noWater	0.406	0.244	0.147	0.271	0.433	0.091
FL	0.261	0.352	0.257	0.385	0.142	0.157
AV	0.119	0.110	0.397	0.383	0.396	0.390
VA	0.103	0.109	0.375	0.369	0.374	0.363
VV	0.094	0.097	0.375	0.365	0.370	0.366

In conclusion, the stress-strain methodology is better suited to be applied in fluxional systems due to the fact that stress response is more sensible to small deformations as we presented above, producing appreciable changes in the stress matrix of several orders of magnitude with respect to the reference stress matrix and it is thus capable of amplify the response of the fluxional crystal towards small distortions.

Alignment of the hydrogen bond network

The orientation of hbs with respect to the principal lattice vectors, is estimated calculating the angle θ_i formed between a vector that goes from the acceptor atom to the proton, and the principal lattice vectors. In Figure 2 it is shown the distribution of the θ_i values for these hbs. In such figure it is clearly seen that the majority of the hbs form large angles with the lattice vectors. The best aligned hbs are considered to be the ones with the smallest θ_i value on each systems, which is found to correspond to hbs in which $\theta_i < 40°$.

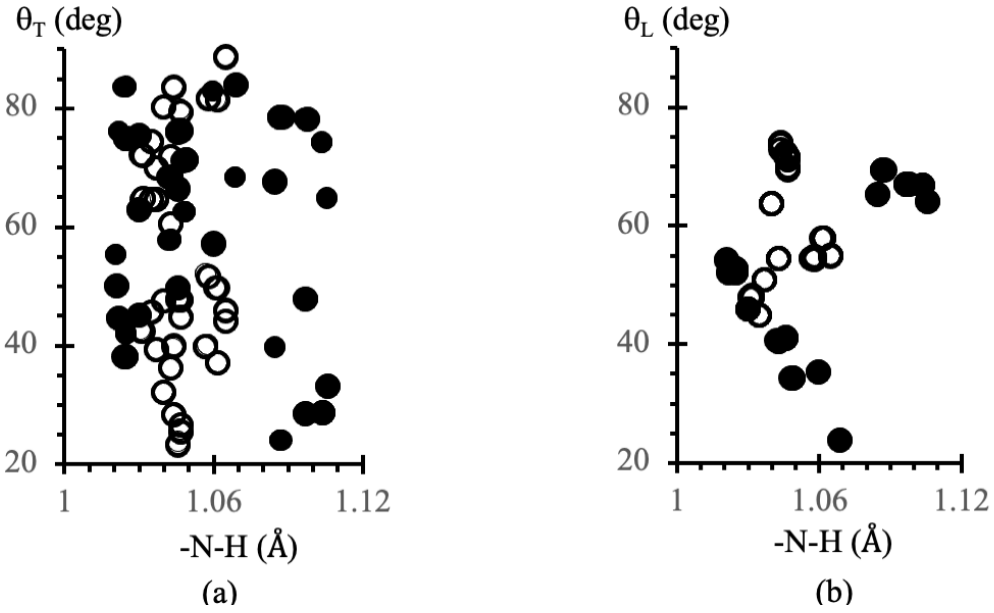

Figure 2: The orientation of hbs with respect to the principal lattice vectors, measured by the θ angle, versus the N-H bond length of the group forming the hbs. (a) Orientation with respect to the lattices vectors perpendicular to the pore axis. (b) Orientation with respect to the lattice vector along the pore axis. Closed circles type F-F crystals. Open circles type V-A crystals.

References

[1] I. Azuri, L. Adler-Abramovich, E. Gazit, O. Hod, and L. Kronik, *Why are diphenylalanine-based peptide nanostructures so rigid? Insights from first principles calculations*, J. Am. Chem. Soc., 136 (2014), pp. 963–969.

[2] M. A. Caro, S. Schulz, and E. P. O'Reilly, *Comparison of stress and total energy methods for calculation of elastic properties of semiconductors*, J. Phys. Condens. Matter, 25 (2012), p. 025803.

[3] M. de Jong, W. Chen, T. Angsten, A. Jain, R. Notestine, A. Gamst, M. Sluiter, C. Krishna Ande, S. van der Zwaag, J. J. Plata, C. Toher, S. Curtarolo, G. Ceder, K. A. Persson, and M. Asta, *Charting the complete elastic properties of inorganic crystalline compounds*, Sci. Data, 2 (2015), p. 150009.

[4] S. P. Ong, W. D. Richards, A. Jain, G. Hautier, M. Kocher, S. Cholia, D. Gunter, V. L. Chevrier, K. A. Persson, and G. Ceder, *Python Materials Genomics (pymatgen): A robust, open-source python library for materials analysis*, Comput. Mater. Sci., 68 (2013), pp. 314–319.